International Journal of Pharmaceutics: X 3 (2021) 100084

Contents lists available at ScienceDirect

International Journal of Pharmaceutics: X

journal homepage: www.sciencedirect.com/journal/international-journal-of-pharmaceutics-x

Towards predicting the product quality in hot-melt extrusion: Pilot plant scale extrusion

Josip Matić [a], Carolina Alva [a], Simone Eder [a], Kathrin Reusch [b], Amrit Paudel [a,c], Johannes Khinast [a,c,*]

[a] Research Center Pharmaceutical Engineering GmbH, Inffeldgasse 13, 8010 Graz, Austria
[b] Leistritz Pharma Extrusion, Markgrafenstraße. 29-39 1, 90459 Nürnberg, Germany
[c] Institute for Process and Particle Engineering, Graz University of Technology, Inffeldgasse 13, 8010 Graz, Austria

ARTICLE INFO

Keywords:
Pharmaceutical HME
Mechanistic modelling
Scale-up
Product quality prediction
Pilot plant scale
ZSE18

ABSTRACT

Following our study on the impact of hot melt extrusion (HME) process conditions on the product quality, we expanded our investigation to assessing the effect of scale-up on the product quality. To this end, we studied the influence of process settings and different scale-up variants on the active pharmaceutical ingredient (API) degradation in a pilot plant scale extruder. Six scale-up variants were investigated and none of them could replicate the product quality from the original process setup on a lab-scale extruder. By analyzing several process-dependent and -independent variables and cross referencing them to the experiments in the lab-scale extruder, we identified certain patterns. The results of the reduced order mechanistic 1D HME simulation of various process states made it possible to establish a correlation between the achieved API degradation and the local melt temperature and the exposure time in specific zones along the screw configuration. Since the same melt temperature and exposure time correlations were also valid for the lab scale-extruder, such an approach could be used in the future to predict the product quality as a function of processing conditions fully in silico prior to the first extrusion trials.

1. Introduction

Turning continuous manufacturing into the main production route of pharmaceuticals is one of the tasks that the U.S. Food and Drug Administration (FDA) and the European Medicines Agency (EMA) are pursuing in an effort to increase both, the production efficiency and the product quality. The Quality by Design (QbD) guidelines(Gupta and Khan, 2012; ICH Q8, 2017; Islam et al., 2014; Kumar and Gupta, 2015; Mishra et al., 2018; Yu et al., 2014) emphasize understanding the product's ingredients, formulation and production steps to intrinsically guarantee a certain product quality.

Used in the polymer and food industries for decades, hot-melt extrusion (HME) is a continuous manufacturing process, often used for mixing of various highly viscous components. The equipment of choice to facilitate the process is usually a closely intermeshing (self-wiping) co-rotation twin-screw extruders (TSE) (Kohlgrüber, 2007; Kolter et al., 2012; Rauwendaal, 2014). The equipment is known for its flexibility in terms of process setup, allowing a formulation-specific process tailored by adjusting the screw configuration and speed, the barrel temperature profile, as well as feeding, venting and strand-shaping. Importantly, the process is solvent-free and ensures both, distributive and dispersive mixing, guaranteeing a good content uniformity. HME is often used for enhancing the solubility of poorly soluble active pharmaceutical ingredients (APIs) (Crowley et al., 2007; McFall et al., 2019; Repka et al., 2018, 2007; Schittny et al., 2018; Vasoya et al., 2019) by creating amorphous solid dispersions or solutions of the API in a polymeric carrier. Alternately, the solubility enhancement can be achieved by creating nanoparticles that are then incorporated into a polymeric carrier via HME (Baumgartner et al., 2016, 2014; Bhagurkar et al., 2017; Khinast et al., 2013; Patil et al., 2015; Silva et al., 2018). In such cases, HME is a one-step solidification process that transforms the liquid nanosuspension into a solid dosage form, with the nano-sized API being embedded in a polymer matrix that guarantees the redispersion of nanoparticles once administered. Moreover, HME has been applied in the production of more traditional embedding of crystalline APIs and peptides in various polymer matrixes (Bode et al., 2019; Cossé et al.,

* Corresponding author at: Institute for Process and Particle Engineering, Graz University of Technology, Inffeldgasse 13/3, A-8010 Graz, Austria.
E-mail address: khinast@tugraz.at (J. Khinast).

https://doi.org/10.1016/j.ijpx.2021.100084
Received 16 May 2021; Accepted 17 May 2021
Available online 6 June 2021

2017; Eder et al., 2017; Koutsamanis et al., 2019). Depending on the polymer matrix and the HME process setup, immediate- or extended-release drug product can be manufactured (Fukuda et al., 2006; Koutsamanis et al., 2020; Vo et al., 2016; Zhu et al., 2006). As a production step, HME can significantly alter the critical quality attributes (CQAs) of the drug product, depending on the used process settings. Even small differences in the thermomechanical load history the formulation experiences during processing can result in seemingly unexplainable product quality differences in the final (or intermediate) product. This is especially true during scale-up where small differences in the melt temperature along the screw configuration can have a significant impact on the solid state of the polymer-API-additive mixture and thus, on the biopharmaceutics. Unfortunately, the impact that certain changes in the process setup or equipment scale can have on the final product are often not known a priory. Nevertheless, these impacts are encountered during process development and routine manufacturing – in the worst case; they might yield a product that does not meet the specifications. Hence, to ensure rapid, cost-efficient and low-risk drug product and process development, a holistic approach has to be established, including defining the intended biopharmaceutical profile and understanding formulation development, production technologies, drug release mechanisms and pharmacokinetics. In this study we focus on the process setup, control and scale-up, using a combination of QbD and in silico tools.

In the past, we have worked on the development of rapid formulation screening tools via vacuum compression molding (Eder et al., 2017; Treffer et al., 2015), high-fidelity simulations based on Smoothed Particle Hydrodynamics (SPH) (Bauer et al., 2020; Eitzlmayr et al., 2014a, 2017; Eitzlmayr and Khinast, 2015b; Ellero and Tanner, 2005; Gingold and Monaghan, 1977, 1982; Monaghan, 2005, 2012; Morris et al., 1997) and 1D HME mechanistic models (Eitzlmayr et al., 2014b, 2013) for HME process analysis, design and scale-up (Baumgartner et al., 2016; Matić et al., 2020b, 2020a, 2019). The current study is a follow up of the experiments, simulations and analyses that were earlier performed using the Leistritz 12 mm ZSE12 HP-PH extruder (Matić et al., 2020a). Six scale-up approaches reported in literature were analyzed by determining the resulting product quality (in terms of API degradation level), comparing the outcomes to the desired product quality and creating detailed 1D HME process simulations. The 1D HME simulations were used to obtain process values that are not possible to be measured experimentally. This includes the melt temperature distribution along the screw configuration, averaged melt temperature across a certain screw section (i.e. kneading section) and the local mean residence time at those screw sections. This allowed us to put the resulting API degradation in correlation with traditional process control values like the process torque, specific mechanical energy consumption or overall mean residence time; but also in correlation with local melt temperature peaks along the screw configuration and local mean residence times, as will be seen in the results section. A similar approach was already explained in our previous study on the extrusions performed on the small-scale ZSE12 extruder (Matić et al., 2020a). The target extruder chosen for this study was the Leistritz 18 mm ZSE18 HP-PH pilot-plant-scale pharma extruder. In addition to the six scale-up attempts, a quasi-DoE setup of nine extrusions (three throughput and screw speed settings) was performed and analyzed in detail to fully understand the process space.

2. Materials and methods

2.1. Simulation approach

Two different simulation approaches were used to support in this study. First, the individual screw elements that assemble the screw configuration were analyzed and parametrized using the Smoothed Particle Hydrodynamics (SPH) simulation approach. The used solver is a weekly compressible SPH solver described in more detail in (Monaghan, 2000, 1994, 1992; Monaghan and Kajtar, 2009), and implemented in our in house developed particle solved XPS (eXtenden Particle System) (Jajcevic et al., 2013; Kureck et al., 2019; Siegmann et al., 2017; Toson et al., 2018). This approach was applied before in our previous work (Bauer et al., 2020; Eitzlmayr et al., 2017, 2014a; Eitzlmayr and Khinast, 2015a, 2015b; Matić et al., 2019) and used to characterize the dimensionless pressure and power characteristics of the investigated screw element pairs. The dimensionless pressure characteristics is defined as the relation between the dimensionless throughput and dimensionless pressure build-up capacity of the screw element pair. Likewise, the power characteristics is defined as the ration between the dimensionless throughput and dimensionless power consumption of the investigated screw element pairs. More information on the dimensionless analysis of individual screw element pairs can be found in our previous publications indicated above and in (Kohlgrüber, 2007; Pawlowski, 1971). The data obtained from the SPH simulations of individual screw element pairs is then used in a second step to parametrize the in house developed reduced order 1D HME code. The 1D HME code is based on a series of mass and energy balance equations which calculate the melt flow inside the extruder, the filling degree, melt temperature along the screw, specific mechanical energy consumption, local and overall residence time distribution. More details can be found in (Eitzlmayr et al., 2014b, 2013; Matić et al., 2020a, 2019).

2.2. Equipment and scale-up rules

The Leistritz ZSE18 pharma extruder is the next bigger extruder after the ZSE12 in the Leistritz pharma extruder lineup. It is often used in pilot plants or even in production lines, depending on the production size needed. The general data for the ZSE18 is shown in Table 1 with a direct size comparison to the smaller ZSE12 extruder, whereas Figure 1 shows the general twin-screw extruder cross section. Both extruders have the same ratio of 1.51 between their outer and inner screw diameters, making the screw transfer and scale-up easier. At the time of our investigations, the ZSE12 extruder had a fixed screw configuration consisting of three conveying elements with pitches of 10, 16 and 20 mm ($C10_{12}$, $C16_{12}$ and $C20_{12}$, respectively) and three kneading elements with angles between the kneading discs of 30, 60 and 90° ($K30_{12}$, $K60_{12}$ and $K90_{12}$, respectively). A broader portfolio of screw elements is available for the ZSE18 extruder. It includes four conveying elements with pitches of 10, 15, 20 and 30 mm ($C10_{18}$, $C15_{18}$, $C20_{18}$ and $C30_{18}$, respectively), one mixing element with a pitch of 15 mm ($M15_{18}$) and six kneading elements with three kneading disc angles of 30, 60 and 90 ($K30_{18}$, $K60_{18}$ and $K90_{18}$, respectively). In addition, the kneading elements can have two disc thicknesses of 4 and 6.5 mm (a kneading element with the thick kneading discs is marked with the letter L, i.e., $K30L_{18}$).

The first step in scaling up the HME process is to transfer the screw configuration. With that regard, the screw configuration was scaled with some guidelines in mind:

- the original screw configuration used during the extrusions on the ZSE12 extruder can be divided into eleven functional sections;
- the sections were created based on the processing tasks and screw groups, with the goal of directly replicating the screw sections to the new target extruder;

Table 1
General characteristics of Leistritz lab-scale 12 mm ZSE12 HP-PH extruder and the pilot-plant-scale 18 mm ZSE18 HP-PH extruder.

	ZSE12 HP-PH	ZSE18 HP-PH
D – Barrel diameter	12 mm	18 mm
D_o – Outer screw diameter	11.85 mm	17.8 mm
D_i – Inner screw diameter	7.85 mm	11.8 mm
Cl – Centerline distance	10 mm	15 mm
τ_{max} – Maximal available torque	20 Nm	71 Nm

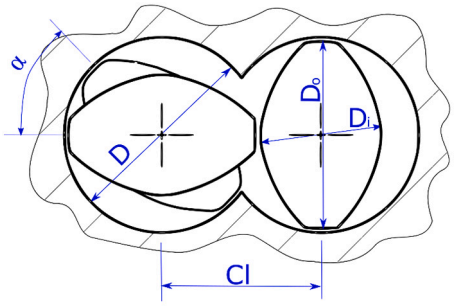

Fig. 1. Details of the twin-screw extruder screw cross-section showing the barrel diameter (D), the screw's outer and inner diameters (Do and Di, respectively), the screw's centerline distance (Cl) and the angle between the kneading discs of the kneading elements (α). Reproduced from (Matić et al., 2020a), with permission.

- to ensure proper section lengths, a ratio of 1.51 was used to scale the section length, which is the ratio between the nominal screw diameters of the target and original extruders.
- the kneading sections were scaled up taking into account the kneading section length, angle between the kneading discs and the kneading element disc thickness;
- some conveying element parts of the screw configuration had to be adjusted due to an insufficient number of screw elements available. In some locations, a conveying element with a pitch of 20 mm was replaced by a conveying element with a pitch of 30 mm. This change was not significant and should not critically affect the performance of the screw configuration.

Both, the original and the target screw configurations are shown in Fig. 2, Table 2 and Table 3. Both screws have the same processing zones and nominal zone lengths, with a relatively complex screw configuration setup. The powder intake zone consists of a long conveying element section with a pitch of 30 mm, and a pitch reduction towards the first kneading zone to 20 mm. The use of high-pitched conveying elements in the powder intake zone is advantageous, as it results in a high free volume, which allows for the intake of different powders, or powder mixtures, with various densities. The pitch reduction of the conveying element towards the first kneading zone is to densify the powder, thereby eliminating any air pockets, and increasing the filling degree before the first kneading zone. The first kneading zone, also known as the melting zone, is a combination of a kneading element with a stagger angle of 30° between individual kneading discs and a 60° kneading element. Such an arrangement results in a soft stagnant zone, since the 60° kneading element has a lower conveying capacity than the 30° kneading element. The second kneading zone is created using an aggressive 90° kneading element that guarantees a fully-filled zone. The next two kneading zones feature a combination of 30° and 60° kneading elements and a single 60° kneading element. This type of setup is typically used to process more complex formulations and involves additional powder or liquid feeding between the kneading sections. Towards the die section an assembly of different conveying elements is used, with a descending pitch from 30 to 20 and finally to 15 mm.

In contrast to the extrusions performed on the ZSE12 extruder (Matić et al., 2020a), for the ZSE18 only one barrel temperature profile setup was chosen, with a maximal barrel temperature of 120 °C in the processing zone. The effect of barrel temperature on the product quality was well addressed in our previous study (Matić et al., 2020a) and is thus, not included in the current investigations. Two settings from the previous ZSE12 extrusions were chosen for the scale-up tests: the PN 2 setting (0.4 kg/h@100 rpm yielding 3.4% API degradation) and the PN 9 setting (0.1 kg/h@500 rpm yielding 60.7% API degradation). These two settings represent the lowest and highest level of API degradation we found for the ZSE12 extruder. In the scale-up trials, six scale-up suggestions were investigated with nine additional extrusions acting as a quasi-DoE setup (Douroumis, 2012; Kohlgrüber, 2007; Rauwendaal, 2014). The scale-up variants are based on two principles:

- geometric similarity with some kind of proportionality factor (five of the scale-up setups, e.g., to keeping mixing or heat-transfer times constant)
- π-theorem theory (one scale-up setup).

The basic assumption behind the scaling process settings in the traditional approach is that with the correct scaling parameters the process state will also be correctly transferred from the original to the target scale. All setups that involve geometric similarity have the same basic form:

$$\frac{Y_2}{Y_1} = \left(\frac{D_2}{D_1}\right)^x \tag{1}$$

where x is the scale exponent, D_1 and D_2 are the nominal diameters of the original and target extruder (the ratio in brackets being 1.51), respectively. Y_1 and Y_2 are the transferred variables, such as screw speed, throughput or torque, of the original and target extruder, respectively. Scale exponent x is used as a scaling factor between the original and target extruder, as shown in Table 4. The scale-up approach based on the π-theorem by Menges and Feistkorn was described in one of our previous papers (Matić et al., 2019) and in (Menges et al., 1983;

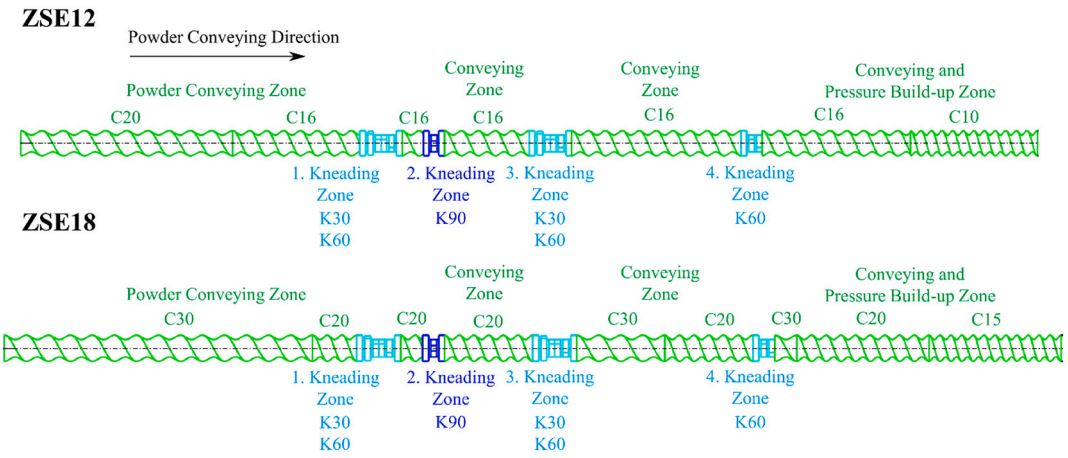

Fig. 2. Screw configuration in the ZSE12 (Matić et al., 2020a) and the ZSE18 extruders for experiments and 1D HME simulations. Reproduced from Matić et al. (2020a), with permission.

Table 2
Screw configuration used in the ZSE12 extrusions (Matić et al., 2020a).

ZSE12 screw configuration					
Name	Screw pitch/ Stagger angle	Cumulative length	Length norm.	Length norm. sum	Section
	[mm/°]	[mm]	[−]	[−]	
GFF-2-20-30	20	30	2.50	2.50	1
GFA-2-20-30	20	60	2.50	5.00	
GFA-2-20-30	20	90	2.50	7.50	
GFA-2-20-10	20	100	0.83	8.33	
GFA-2-16-20	16	120	1.67	10.00	2
GFA-2-16-20	16	140	1.67	11.67	
GFA-2-16-20	16	160	1.67	13.33	
KB4–2–10-30°-*Re*	30°	170	0.83	14.17	3
KB4–2–10-60°-*Re*	60°	180	0.83	15.00	
GFA-2-16-10	16	190	0.83	15.83	4
KB4–2–10-90°	90°	200	0.83	16.67	5
GFA-2-16-20	16	220	1.67	18.33	6
GFA-2-16-20	16	240	1.67	20.00	
KB4–2–10-30°-*Re*	30°	250	0.83	20.83	7
KB4–2–10-60°-*Re*	60°	260	0.83	21.67	
GFA-2-16-20	16	280	1.67	23.33	8
GFA-2-16-20	16	300	1.67	25.00	
GFA-2-16-20	16	320	1.67	26.67	
GFA-2-16-20	16	340	1.67	28.33	
KB4–2–10-60°-*Re*	60°	350	0.83	29.17	9
GFA-2-16-20	16	370	1.67	30.83	10
GFA-2-16-20	16	390	1.67	32.50	
GFA-2-16-20	16	410	1.67	34.17	
GFA-2-16-10	16	420	0.83	35.00	
GFA-2-10-20	10	440	1.67	36.67	11
GFA-2-10-20	10	460	1.67	38.33	
GFA-2-10-20	10	480	1.67	40.00	

Menges and Feistkorn, 1984). Here, the basis for the scale-up is also given in eq. (1), with the difference that the scaling exponents are determined based on π quantities. The different π quantities are based on the specific drive power, specific heat capacity, pressure build-up, mixing effect, heat transfer and thermal homogeneity. By rearranging the different π quantities, different relations between the *Y* and *D* variables (eq. 1) can be created with the scale exponend x determined by the π quantities. The resulting process settings are shown in Table 5. Compared to the original settings, a combination of the same or higher throughput and the same or lower screw speed was calculated from the different scale-up laws.

Table 3
Screw configurations used in the ZSE18 extrusions.

ZSE18 screw configuration					
Name	Screw pitch/ Stagger angle	Cumulative length	Length norm.	Length norm. sum	Section
	[mm/°]	[mm]	[−]	[−]	
GFF-2-30-90	30	90	5.00	5.00	1
GFA-2-30-60	30	150	3.33	8.33	
GFA-2-30-60	20	210	3.33	11.67	2
GFA-2-20-30	20	240	1.67	13.33	
KB-4-2-15-30°-*Re*	30°	255	0.83	14.17	3
KB-4-2-15-60°-*Re*	60°	270	0.83	15.00	
GFA-2-20-15	20	285	0.83	15.83	4
KB-4-2-15-90°	90°	300	0.83	16.67	5
GFA-2-20-60	20	360	3.33	20.00	6
KB-4-2-15-30°-*Re*	30°	375	0.83	20.83	7
KB-4-2-15-60°-*Re*	60°	390	0.83	21.67	
GFA-2-30-30	20	450	3.33	25.00	8
GFA-2-30-30	20	480	1.67	26.67	
GFA-2-20-60	20	510	1.67	28.33	
KB-4-2-15-60°-*Re*	60°	525	0.83	29.17	9
GFA-2-30-15	20	555	1.67	30.83	10
GFA-2-20-30	20	585	1.67	32.50	
GFA-2-20-30	20	615	1.67	34.17	
GFA-2-20-30	20	630	0.83	35.00	
GFA-2-15-30	15	660	1.67	36.67	11
GFA-2-15-30	15	690	1.67	38.33	
GFA-2-15-30	15	720	1.67	40.00	

Table 4
Values of the x-scaling exponent used for the scale-up rules based on the geometry similarity between the ZSE12 and ZSE18 extruders.

	C	HT	M	R1	R2
n [rpm]	−0.5	−1	0	−0.769	−1
m [kg/h]	2	1.5	3	0	0.5

All scale-up variations shown in Table 5 span only a limited design space. Hence, in addition to the obtained process settings, nine DoE runs were performed to cover a throughput ranging from 0.5 to 1 and 1.5 kg/h and a screw speed ranging from 100 to 200 and 300 rpm. The goal of these additional settings was to explore a wider operating space.

Table 5
Process parameters used for the scale-up runs and DoE in the ZSE18 target extruder. ZSE12 settings: 0.4 kg/h with a screw speed of 100 rpm (resulting API degradation of 3.4%) and 0.1 kg/h with a screw speed of 500 rpm (resulting API degradation of 60.7%).

	Process settings	m [kg/h]	n [rpm]	API Deg.
Literature scale-up	R1–1	0.4	73	10.6%
	R1–2	0.1	366	100.0%
	R2–1	0.5	67	9.0%
	R2–2	0.1	333	100.0%
	C1	0.9	82	5.2%
	C2	0.2	408	100.0%
	HT-1	0.7	67	7.8%
	HT-2	0.2	333	100.0%
	M-1	1.4	100	5.5%
	M-2	0.3	500	100.0%
	Meng1	0.8	100	8.1%
	Meng2	0.2	500	100.0%
DoE settings	DoE-1.1	0.5	100	9.5%
	DoE-1.2	0.5	200	39.4%
	DoE-1.3	0.5	300	60.0%
	DoE-2.1	1	100	7.8%
	DoE-2.2	1	200	17.1%
	DoE-2.3	1	300	28.8%
	DoE-3.1	1.5	100	5.3%
	DoE-3.2	1.5	200	11.5%
	DoE-3.3	1.5	300	19.4%

2.3. Formulation, API degradation and residence time distribution measurements

The investigated formulation was a simple two-component system with an 80% mass loading of Eudragit RL PO and a 20% mass loading of famotidine. Importantly, famotidine is known to be prone to degradation right after melting (Chordiya et al., 2011; Maniruzzaman et al., 2013; Mustafin, 2011; Parikh et al., 2014; Perpétuo et al., 2013; Viciosa et al., 2016). Hence, API degradation was expected during extrusion and was used as a quality attribute. Samples were collected during the extrusions and the amount of API degraded was determined offline via ultra-high performance liquid chromatography (UPLC). Triplicates of randomly-sampled pellets were weighed in volumetric flasks and dissolved in methanol in an ultrasound bath for 10 min. The resulting solutions were transparent, ranging from colorless to red, correlating with the extrudate's color. This suggests that the impurity responsible for the color may be soluble in methanol. The percent of degradation f was calculated based on the difference between initial pre-blend content C_0 and final extrudate content $C_{extrudate}$ from the UPLC measurements.

$$f = \frac{C_0 - C_{extrudate}}{C_0} \cdot 100\% \tag{2}$$

The content of Famotidine from the extrudates Famotidine solutions was obtained via UPLC using an Acquity UPLC™ HSS T3 (100 × 2.1 mm^2) 1.8-µm column at 40 °C and a detection wavelength of 266 nm. Gradient elution was applied to separate FAM from its impurities, with a mobile phase of ACN (acetronytril) and TFA (trifluoroacetic acid) in water, a variable composition over time and a constant flow rate of 0.4 mL/min. For more details, the reader is refer to (Matić et al., 2020a).

The residence time distribution (RTD) of the process was measured and used as a critical process parameter important for understanding the process state and its connection to the product quality, similar to the specific mechanical energy consumption (SMEC). A blue pigmented tracer pellet of approximately 10-20 mg was inserted into the extruder's powder inlet. At the same time a camera (Fujifilm Fine Pix HS25EXR) began recording the die's strand outlet. The resulting videos were post-processed in Matlab® (Mathworks, Natick, MA, USA) using the script developed earlier (Kruisz et al., 2018, 2017; Wahl et al., 2018). Each video frame was analyzed to determine the average values assigned to the RGB color space within a specified mask, which deliberately included only the portion of strand where the color change was observed. For a better signal, the score of 1st Principal Components (PC1) of RGB values was computed and accessed. The PC1 signals obtained were fitted to an analytical solution of the Fokker-Planck equation for twin-screw extruders, where the exit age distribution $E(\tau)$ is a function of the Peclet number Pe and the dimensionless time $\tau = t/\theta$, with t being the actual time and θ being the mean residence time (mRT):

$$\text{color values} = k\, f(Pe, \tau) \tag{3}$$

$$E(\tau) = f(Pe, \tau) = \sqrt{\frac{Pe}{\pi\tau}} exp\left(-\frac{Pe}{4}\frac{(1-\tau)^2}{\tau}\right) - \frac{Pe}{2} exp(Pe)\, erfc\left(\sqrt{\frac{Pe}{4}}\frac{1+\tau}{\sqrt{\tau}}\right) \tag{4}$$

3. Results and discussion

During the experimental runs, the dependent process values, such as the torque, the specific mechanical energy consumption (SMEC) and the RTD, were monitored and characterized. The obtained results were compared to in silico obtained results of the same process settings using our 1D HME software developed in-house. These are in good agreement, as shown in Fig. 3 to Fig. 5.

In the context of scale-up, it is interesting to compare the change of the dependent process variables as a function of the scale-up (i.e., the expected change in the values for a given extruder size difference). These results are summarized in Table 6. The obtained torque values from the ZSE18 experiments are all clustered around 30 Nm value. Considering that for the process settings PN 2 (0.4 kg/h@100 rpm) and PN 9 (0.1 kg/h@500 rpm) of the original ZSE12 extruder, a torque of 4.3 and 3.6 Nm was needed for processing, the torque required for equivalent processing on the ZSE18 was around 7 times higher, while the screw diameter was only 1.5 times larger. This is important for proper equipment selections during scale-up, as equipment might have torque limitations. In addition to the process torque, the process SMEC was evaluated and compared to the values obtained in silico (Fig. 4). The SMEC is calculated based on the process torque, throughput and screw speed as follow:

$$SMEC\ [kWh/kg] = \frac{2 \cdot \pi \cdot n[rpm] \cdot \tau[Nm]}{60000 \cdot \dot{m}[kg/h]} \tag{5}$$

Overall, the resulting SMEC values for the ZSE18 were higher compared to the original PN2 and PN9 case and greatly varied as a function of the scale-up method (i.e., 0.25–0.54 kWh/kg and 4.1–10.6 kWh/kg), compared to the original 0.11 kWh/kg (PN2 case) and 1.88 kWh/kg (PN9 case). This indicates that similar to the torque, after scale-up, the SMEC increases by a factor of 2 to 5. This is of great importance, since the SMEC mostly contributes to the viscous dissipation and thus, to the increase in melt temperature. Additionally, considering that the

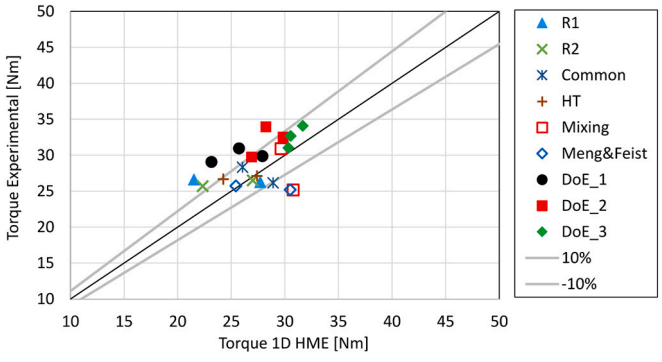

Fig. 3. Comparison between the in silico and experimentally obtained torque values from the scale-up and DoE extrusion in the ZSE18 extruder.

Table 6
Comparison between the torque, SMEC and mRT values for two process settings of the original extruder (PN 2 and PN 9 of ZSE12) and their corresponding scale-up settings of the target extruder (ZSE18), with calculated relative change values.[a]

ZSE12	ZSE18	n	m	Torque ZSE12	Torque ZSE18	Relative change	SMEC ZSE12	SMEC ZSE18	Relative change	mRT ZSE12	mRT ZSE18	Relative change
		[rpm]	[kg/h]	[Nm]	[Nm]	[−]	[kWh/kg]	[kWh/kg]	[−]	[s]	[s]	[−]
PN 2 (0.4 kg/h@100 rpm)	R1–1	73	0.4	4.3	28.1	6.6	0.11	0.54	4.8	164	425	2.6
	R2–1	67	0.5		27.1	6.4		0.39	3.5		346	2.1
	C1	82	0.9		29.9	7.0		0.28	2.5		230	1.4
	HT-1	67	0.7		28.1	6.6		0.27	2.4		284	1.7
	M-1	100	1.4		32.6	7.7		0.25	2.3		143	0.9
	Meng1	100	0.8		27.2	6.4		0.36	3.2		215	1.3
PN 9 (0.1 kg/h@500 rpm)	R1–2	366	0.1	3.6	27.7	7.7	1.88	10.61	5.6	498	1475[a]	3.0
	R2-2	333	0.1		28.0	7.8		7.95	4.2		1476[a]	3.0
	C2	408	0.2		27.6	7.7		5.23	2.8		741[a]	1.5
	HT-2	333	0.2		28.6	8.0		5.42	2.9		743[a]	1.5
	M-2	500	0.3		26.5	7.4		4.10	2.2		495[a]	1.0
	Meng2	500	0.2		26.6	7.4		6.96	3.7		739[a]	1.5

[a] obtained via 1D HME simulation.

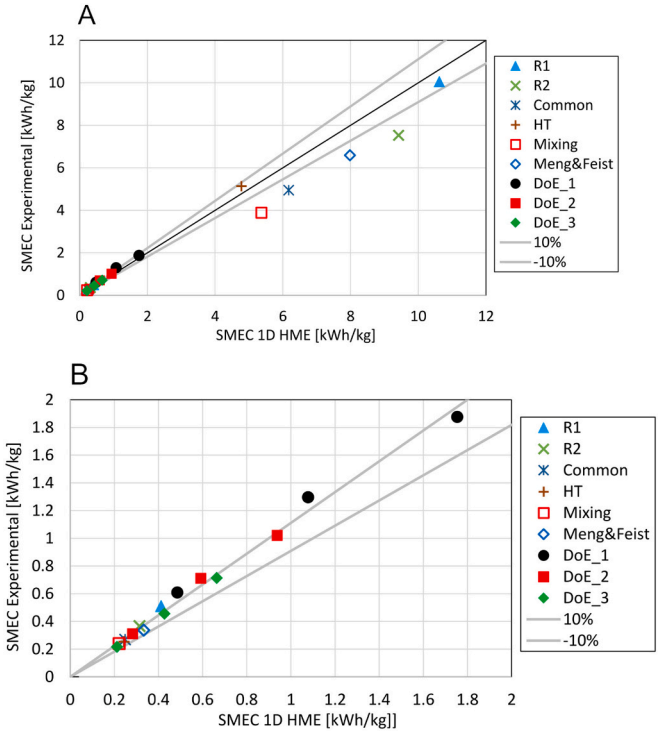

Fig. 4. Comparison between the in silico and experimentally obtained SMEC values from the scale-up and DoE extrusion in the ZSE18 extruder. Top figure (fig. A) shows the SMEC values from 0 to 12 kWh/kg, and bottom figure (fig. B) shows a zoomed in view with SMEC values from 0 to 2 kWh/kg.

increase in the available surface area for efficient melt cooling (scales with square power of the size) is lower compared to the available material in a certain location that requires cooling (scales cubically), higher overall melt temperatures can be expected in the ZSE18 compared to the ZSE12.

In addition, the mean residence time (mRT) was evaluated and compared to the values obtained in silico, (Fig. 5). Similar to the torque and the SMEC, the mRT changed as a result of scale-up. Having a mRT of 164 s at small scale (PN2 case), the mRT values in the target extruder ranged from 140 s to 420 s, resulting in a difference of 0.85 to 2.6. Likewise, for the PN9 case, the small-scale mRT was 498 s and the large-scale mRT ranged between 495 and 475 s, which is 1 to 3 times longer

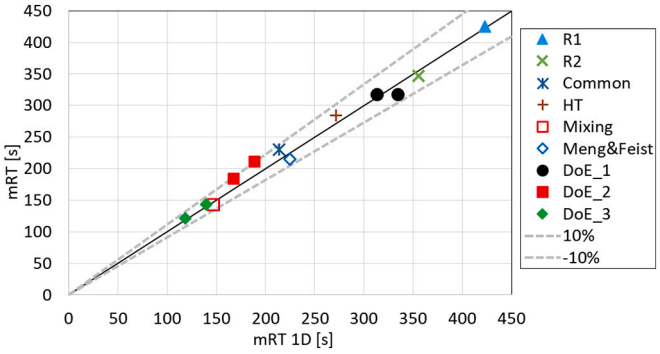

Fig. 5. Comparison between the in silico and experimentally obtained mean RTD values from the scale-up and DoE extrusion in the ZSE18 extruder.

mRT. In line with the analysis of the SMEC values, this indicates that -in addition to higher expected melt temperatures - on average the formulation is subjected to longer process times.

The observed API degradations were analyzed as a function of process settings and dependent process variables and were compared to the originally achieved API degradations in the ZSE12. Table 5 and Fig. 6 show the small-scale process settings and API degradation points of the ZSE12 extruder, as well as the process settings obtained using the various scale-up approaches and the DoE settings of the target ZSE18 extruder and the corresponding API degradations. As can be clearly seen from the Fig. 6 and Table 5, none of the scale-up options for the ZSE18 resulted in the same degree of API degradation. For the ZSE18 the extent of API degradation ranged from 5.2% to 10.6%, whereas it was only 3.4% in the ZSE12 (PN2, 0.4 kg/h@100 rpm, ZSE12). For the PN9 case (0.1 kg/h@500 rpm) 60.7% of the API was degraded after extrusion in the ZSE12; for the ZSE18 all scale-up scenarios resulted even in complete API degradation. Hence, these findings will not be further analyzed. The DoE settings yielded API degradations from 9.5 to 60% at 0.5 kg/h throughput, from 7.8 to 28.8% at 1 kg/h throughput and from 5.3 to 19.4% at 1.5 kg/h throughput. Fig. 6 (bottom) shows the process settings versus the API degradation derived from the PN2 setup and the nine DoE settings. If only the DoE settings are analyzed, it is clear that for a constant screw speed, barrel temperature and screw configuration an increase in the throughput directly decreases the API degradation. Given that everything except the throughput is kept constant, it can be argued that the prevailing stress state induced on the formulation is also constant since the stress acting on the formulation is a function of screw and barrel geometry parameters and the screw speed. Hence, an increase in

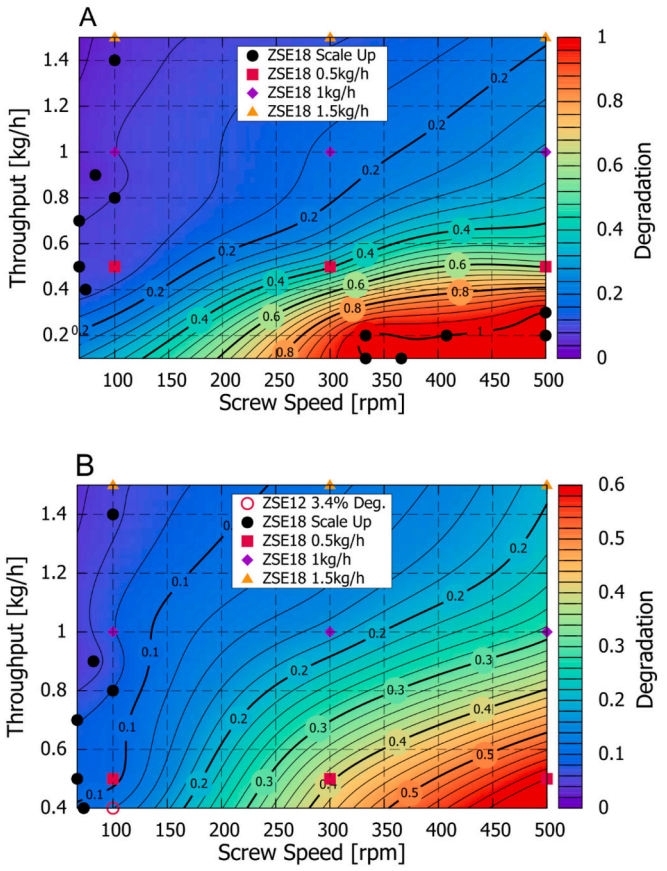

Fig. 6. Process settings and product quality (extent of API degradation in the extrudate) related to various scale-up scenarios in the ZSE18 extruder. Top: Scale-up and DoE settings on the ZSE18 extruder; Bottom: Scale-up and DoE settings on the ZSE18 extruder, only based on the ZSE18 0.4 kg/h@100 rpm-3.4% API Degradation (this figure excludes the settings that resulted with 100% API Degradation).

the throughput reduces the API degradation due to the reduction in the mRT. This is demonstrated in Fig. 7, which shows the achieved API degradation as a function of the overall process mRT_{1D}. Clearly, a reduction in the process throughput results in an increase of the processing time of the formulation (longer mean residence time) and higher overall degradation and spread of achieved API degradations when varying the screw speed. Increasing the process throughput reduces the API degradation levels and the spread of achieved API degradations.

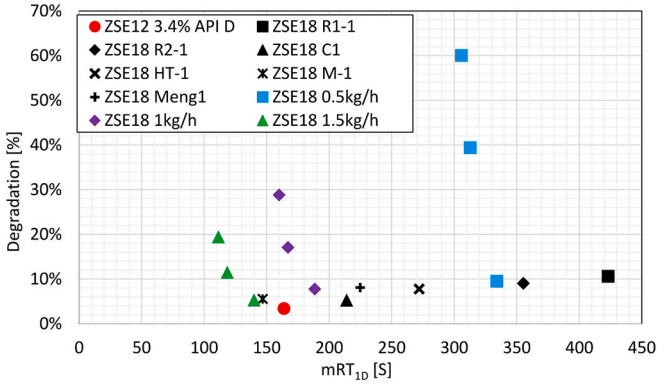

Fig. 7. Achieved API degradation as a function of process mRT_{1D}. Comparison between 0.4 kg/h@100 rpm settings of the original extruder, resulting in a degradation of 3.4%, and the scaled and DoE settings of the target ZSE18 extruder.

Still, as suggested by the results of the scale-up settings, the mean residence time is not an unambiguous process descriptor and cannot be directly connected to the API degradation. Similar API degradations can be achieved at various mean residence times. For example, around 10% API degradation can be achieved with mRT_{1D} values of around 110, 330 and 425 s. Going back to Fig. 6 and the DoE settings, any increase in the screw speed corresponds to an increase in the API degradation. Although an increase in the screw speed also leads to some reduction in the mRT, the mRT does not play the key role in such a scenario. Here, the direct increase in the viscous dissipation caused by a higher screw speed directly results in an increase in the observed API degradation. Comparing the ZSE18 settings to the original setting on the ZSE12 extruder, the data suggest that a one-to-one process transfer (keeping the screw speed and throughput constant, regardless of the extruder size change) is likely to result in an API degradation close to 12%, in comparison to the original 3.4%.

Trying to connect the achieved process SMEC to the observed API degradation one can find similar results as in the case of the mRT (Fig. 8). At first glance, the SMEC linearly correlates with the API degradation, i.e., a higher process SMEC generally resulting in a higher API degradation. However, the correlation is not as clear when most of the available data for API degradations below 12% is examined in detail. Again, multiple points can be found with either a similar SMEC but different resulting API degradations or a similar API degradation achieved at different process SMEC values.

Please note that the above-mentioned results only cover a limited range of process settings, one barrel temperature setting and, more importantly, only one screw configuration. Varying the screw configuration could lead to even bigger issues when trying to connect the API degradation or any other product specific quality attribute to the process

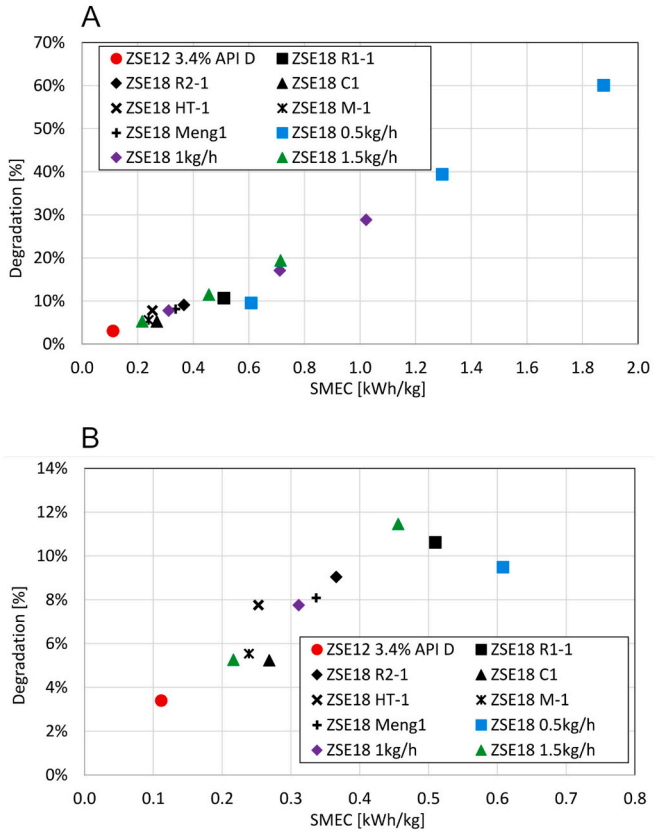

Fig. 8. Achieved API degradation as a function of process SMEC for the small-scale extruder (PN2 case) and the large-scale ZSE18 extruder. Top figure (fig. A) in the full SMEC range from 0 to 2 kWh/kg, bottom figure (fig. B) in the SMEC range from 0 to 0.8 kWh/kg.

dependent or independent variables. Therefore, the SMEC and the mRT cannot be considered unambiguous indicators of expected product quality. This also means that the use of statistics-based analysis, such as those used in typical DoE setups, is limited.

Assuming that the API degradation directly correlates with the melt temperature and the mean residence time in the screw zones, heat maps were created for the different processing zones along the screw configuration. These heat maps show the API degradation as a function of the calculated averaged melt temperature in the analyzed zone and the local mRT_{1D} (i.e. exposure time). The calculated values of the local melt temperature correspond to the melt temperature averaged over the section length and the screw cross section. Here 1D HME simulations were used as the measurement of the melt temperature at specific zones along the screw configuration is not well established. From the DoE data it is clear that an increase in screw speed, for everything else left constant, leads to a direct melt temperature increase in the fully filled zones, in this case in the location of the 90° kneading element. On the other hand, and increase in throughput reduces the local exposure time (lmRT) the processed formulation is subjected to a certain temperature in the fully filled screw zone. The combination of the exposure time and temperature have a good correlation to the observed API degradation. Extrusions performed in the ZSE12 (Matić et al., 2020a) extruder showed that the local melt temperature and the local mRT_{1D} of the harshest kneading element zone with 90° kneading elements correlates best with the achieved API degradation values. The same is true in the case of ZSE18 extrusions, as demonstrated in Fig. 9. On the left side of the Figure, the starting point of the ZSE12 extruder is shown with a local mRT of about 8 s and an average melt temperature of about 158 °C, which resulted in an API degradation of 3.4% in the extrudate. The remaining points in the plot are a result of the scale-up including the DoE settings. Similar to the results of the ZSE12 extrusions, an increase in the exposure time or exposure to a higher melt temperature inevitably leads to an increase in API degradation in the extrudate. This provides a very direct and intuitive link to the expected product quality and offers new possibilities for the process design and scale-up. Such a correlation could be very significant in the process design and scale-up phases. By designing the formulation's heat map (exposure time vs. temperature vs. chosen quality attribute) before the first extrusion experiments, various extruder setups and settings could be investigated fully in silico to provide a first estimate of the expected product quality before any extrusion trials commence. Following this, potential process setups could be tested and evaluated fully in silico without producing waste, and consuming facilities and costs associated with non-GMP and GMP process setups. It should be noted that, although promising, this approach should be tested and further improved using a variety of formulations, product quality attributes, extruders and process setups.

4. Summary and conclusion

This study is a continuation of the previously reported analyses of experiments and simulations for the small-scale ZSE12 twin screw extruder. Our work focuses on correlations between the process settings and the product quality (in this case degradation), as well as on the effect of the extruder size on the product quality. As part of the process transfer from ZSE12 to the ZSE18 extruder, the transfer of the screw configuration was addressed and several scale-up laws were applied. The resulting API degradation was compared to the results.

No scale-up law applied resulted in the same API degradation: in all cases the resulting degree of API degradation was higher compared to the original ones. As part of the analysis, the influence of process independent and dependent variables was analyzed with the goal of finding correlations with the resulting process quality. In line with the previous study, it was established that the API degradation correlates well with the local average melt temperature and the local mean residence time in a certain zone along the screw configuration. In the case of the formulation and screw configuration studied, the 90° kneading element zone

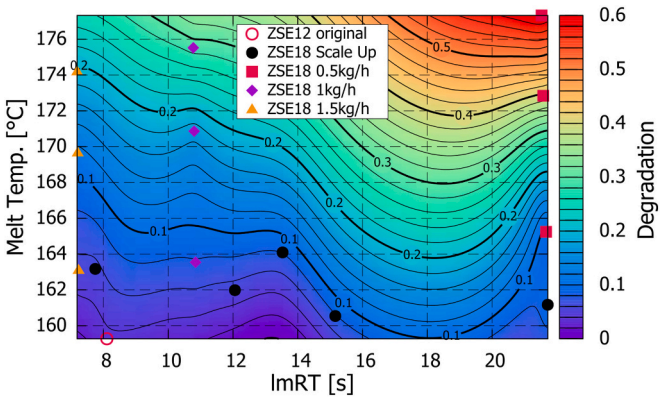

Fig. 9. API degradation as a function of local average melt temperature and local mRT in the 90° kneading element section (at 90° kneading element). Only scale-up results for the small-scale case (PN2 with 3.4% API degradation at 0.4 kg/h and100 rpm) as a basis are shown.

was the most significant one. Note that local values of the melt temperature along the screw configuration and local mean residence times for different sections along the screw configuration are not readily available with current experimental approaches, but are relatively simple to compute with help of different simulation approaches shown here. The above correlation seems to be scale-independent since it was established in both ZSE12 and ZSE18 extrusion studies. This suggests that, rather than focusing on scaling process settings the focus should be on accurately representing the process state and then reproducing the same process state on different scales independent of the process settings or screw configuration. The results indicate the possibility of predicting the product quality in silico prior to any extrusion experiments, provided that a heat map of the formulation can be created showing correlations between the formulation's quality attributes, melt temperature and exposure time. Thus, the process scale-up could be reduced to a simple in silico DoE study on various extruder scales. This would allow the testing of different screw configurations that could lead to a better equivalent product quality at higher yield without material waste. The next steps will be to evaluate this approach and refine it using a variety of formulations, product quality attributes, extruder and process conditions.

Declaration of Competing Interest

None.

Acknowledgement

This work has been funded within the Austrian COMET Program under the auspices of the Austrian Federal Ministry of Transport, Innovation and Technology (bmvit), the Austrian Federal Ministry of Economy, Family and Youth (bmwfj) and by the State of Styria (Styrian Funding Agency SFG). COMET is managed by the Austrian Research Promotion Agency FFG.

References

Bauer, H., Matić, J., Khinast, J., 2020. Characteristic parameters and process maps for fully-filled twin-screw extruder elements. Chem. Eng. Sci. 116202 https://doi.org/10.1016/j.ces.2020.116202.

Baumgartner, R., Eitzlmayr, A., Matsko, N., Tetyczka, C., Khinast, J.G., Roblegg, E., 2014. Nano-extrusion: a promising tool for continuous manufacturing of solid nanoformulations. Int. J. Pharm. 477, 1–11. https://doi.org/10.1016/j.ijpharm.2014.10.008.

Baumgartner, R., Matić, J., Schrank, S., Laske, S., Khinast, J., Roblegg, E., 2016. NANEX: process design and optimization. Int. J. Pharm. 506, 35–45. https://doi.org/10.1016/j.ijpharm.2016.04.029.

Bhagurkar, A.M., Repka, M.A., Murthy, S.N., 2017. A novel approach for the development of a nanostructured lipid carrier formulation by hot-melt extrusion

technology. J. Pharm. Sci. 106, 1085–1091. https://doi.org/10.1016/j.xphs.2016.12.015.
Bode, C., Kranz, H., Fivez, A., Siepmann, F., Siepmann, J., 2019. Often neglected: PLGA/PLA swelling orchestrates drug release: HME implants. J. Control. Release 306, 97–107. https://doi.org/10.1016/j.jconrel.2019.05.039.
Chordiya, M., Gangurde, H., Senthilkumaran, K., Kothari, L., 2011. Formulation development and in vitro evaluation of gastroretentive hollow microspheres of famotidine. Int. J. Pharm. Investig. 1, 105. https://doi.org/10.4103/2230-973x.82423.
Cossé, A., König, C., Lamprecht, A., Wagner, K.G., 2017. Hot melt extrusion for sustained protein release: matrix erosion and in vitro release of PLGA-based implants. AAPS PharmSciTech 18, 15–26. https://doi.org/10.1208/s12249-016-0548-5.
Crowley, M.M., Zhang, F., Repka, M.A., Thumma, S., Upadhye, S.B., Kumar Battu, S., McGinity, J.W., Martin, C., 2007. Pharmaceutical applications of hot-melt extrusion: part I. Drug Dev. Ind. Pharm. 33, 909–926. https://doi.org/10.1080/03639040701498759.
Douroumis, D., 2012. Hot-Melt Extrusion: Pharmaceutical Applications. John Wiley & Sons, Ltd, Chichester, UK. https://doi.org/10.1002/9780470711415.
Eder, S., Beretta, M., Witschnigg, A., Koutsamanis, I., Eggenreich, K., Khinast, J.G., Koscher, G., Paudel, A., Nickisch, K., Friedrich, M., Froehlich, E., Roblegg, E., 2017. Establishment of a molding procedure to facilitate formulation development for co-extrudates. AAPS PharmSciTech 18, 2971–2976. https://doi.org/10.1208/s12249-017-0788-z.
Eitzlmayr, A., Khinast, J., 2015a. Co-rotating twin-screw extruders: detailed analysis of conveying elements based on smoothed particle hydrodynamics. Part 2: mixing. Chem. Eng. Sci. 134, 880–886. https://doi.org/10.1016/j.ces.2015.05.035.
Eitzlmayr, A., Khinast, J.G., 2015b. Co-rotating twin-screw extruders: detailed analysis of conveying elements based on smoothed particle hydrodynamics. Part 1: hydrodynamics. Chem. Eng. Sci. 134, 861–879. https://doi.org/10.1016/j.ces.2015.04.055.
Eitzlmayr, A., Khinast, J.G., Hörl, G., Koscher, G., Reynolds, G., Huang, Z., Booth, J., Shering, P., 2013. Experimental characterization and modeling of twin-screw extruder elements for pharmaceutical hot melt extrusion. AICHE J. 59, 4440–4450. https://doi.org/10.1002/aic.14184.
Eitzlmayr, A., Koscher, G., Khinast, J.G., 2014a. A novel method for modeling of complex wall geometries in smoothed particle hydrodynamics. Comput. Phys. Commun. 185, 2436–2448. https://doi.org/10.1016/j.cpc.2014.05.014.
Eitzlmayr, A., Koscher, G., Reynolds, G., Huang, Z., Booth, J., Shering, P., Khinast, J.G., 2014b. Mechanistic modeling of modular co-rotating twin-screw extruders. Int. J. Pharm. 474, 157–176. https://doi.org/10.1016/j.ijpharm.2014.08.005.
Eitzlmayr, A., Matić, J., Khinast, J.G., 2017. Analysis of flow and mixing in screw elements of corotating twin-screw extruders via SPH. AICHE J. 63, 2451–2463. https://doi.org/10.1002/aic.15607.
Ellero, M., Tanner, R.I., 2005. SPH simulations of transient viscoelastic flows at low Reynolds number. J. Nonnewton. Fluid Mech. 132, 61–72. https://doi.org/10.1016/j.jnnfm.2005.08.012.
Fukuda, M., Peppas, N.A., McGinity, J.W., 2006. Floating hot-melt extruded tablets for gastroretentive controlled drug release system. J. Control. Release 115, 121–129. https://doi.org/10.1016/j.jconrel.2006.07.018.
Gingold, R.A., Monaghan, J.J., 1977. Smoothed particle hydrodynamics: theory and application to non-spherical stars. Mon. Not. R. Astron. Soc. 181, 375–389. https://doi.org/10.1093/mnras/181.3.375.
Gingold, R.A., Monaghan, J.J., 1982. Kernel estimates as a basis for general particle methods in hydrodynamics. J. Comput. Phys. 46, 429–453.
Gupta, A., Khan, M.A., 2012. Hot-Melt Extrusion: An FDA Perspective on Product and Process Understanding. In: Hot-Melt Extrusion: Pharmaceutical Applications. John Wiley & Sons, Ltd, Chichester, UK, pp. 323–331. https://doi.org/10.1002/9780470711415.ch15.
ICH Q8, 2017. EMEA/CHMP, 2009, ICH Topic Q 8 (R2) Pharmaceutical Development, Step 5: Note for Guidance on Pharmaceutical Development 8.
Islam, M.T., Maniruzzaman, M., Halsey, S.A., Chowdhry, B.Z., Douroumis, D., 2014. Development of sustained-release formulations processed by hot-melt extrusion by using a quality-by-design approach. Drug Deliv. Transl. Res. 4, 377–387. https://doi.org/10.1007/s13346-014-0197-8.
Jajcevic, D., Siegmann, E., Radeke, C., Khinast, J.G., 2013. Large-scale CFD–DEM simulations of fluidized granular systems. Chem. Eng. Sci. 98, 298–310. https://doi.org/10.1016/j.ces.2013.05.014.
Khinast, J.G., Baumgartner, R., Roblegg, E., 2013. Nano-extrusion: a one-step process for manufacturing of solid nanoparticle formulations directly from the liquid phase. AAPS PharmSciTech 14, 601–604. https://doi.org/10.1208/s12249-013-9946-0.
Kohlgrüber, K., 2007. Co-Rotating Twin-Screw Extruder, Co-Rotating Twin-Screw Extruders: Fundamentals, Technology, and Applications. Carl Hanser Verlag GmbH & Co. KG, München. https://doi.org/10.3139/9783446433410.
Kolter, K., Karl, M., Gryczke, A., 2012. Hot-melt extrusion with BASF polymers. In: Extrusion Compendium. BASF.
Koutsamanis, I., Eder, S., Beretta, M., Witschnigg, A., Paudel, A., Nickisch, K., Friedrich, M., Eggenreich, K., Roblegg, E., 2019. Formulation and processability screening for the rational design of ethylene-vinyl acetate based intra-vaginal rings. Int. J. Pharm. 564, 90–97. https://doi.org/10.1016/j.ijpharm.2019.04.041.
Koutsamanis, I., Paudel, A., Nickisch, K., Eggenreich, K., Roblegg, E., Eder, S., 2020. Controlled-release from high-loaded reservoir-type systems—a case study of ethylene-vinyl acetate and progesterone. Pharmaceutics 12, 103. https://doi.org/10.3390/pharmaceutics12020103.
Kruisz, J., Rehrl, J., Faulhammer, E., Witschnigg, A., Khinast, J.G., 2018. Material tracking in a continuous direct capsule-filling process via residence time distribution measurements. Int. J. Pharm. 550, 347–358. https://doi.org/10.1016/j.ijpharm.2018.08.056.
Kruisz, J., Rehrl, J., Sacher, S., Aigner, I., Horn, M., Khinast, J.G., 2017. RTD modeling of a continuous dry granulation process for process control and materials diversion. Int. J. Pharm. 528, 334–344. https://doi.org/10.1016/j.ijpharm.2017.06.001.
Kumar, V.P., Gupta, N.V., 2015. A review on quality by design (QBD) for pharmaceuticals. Int. J. Drug Dev. Res. 7, 35–44.
Kureck, H., Govender, N., Siegmann, E., Boehling, P., Radeke, C., Khinast, J.G., 2019. Industrial scale simulations of tablet coating using GPU based DEM: a validation study. Chem. Eng. Sci. 202, 462–480. https://doi.org/10.1016/j.ces.2019.03.029.
Maniruzzaman, M., Rana, M.M., Boateng, J.S., Mitchell, J.C., Douroumis, D., 2013. Dissolution enhancement of poorly water-soluble APIs processed by hot-melt extrusion using hydrophilic polymers. Drug Dev. Ind. Pharm. 39, 218–227. https://doi.org/10.3109/03639045.2012.670642.
Matić, J., Alva, C., Witschnigg, A., Eder, S., Reusch, K., Paudel, A., Khinast, J., 2020a. Towards predicting the product quality in hot-melt extrusion: small scale extrusion. Int. J. Pharm. X 2, 100062. https://doi.org/10.1016/j.ijpx.2020.100062.
Matić, J., Paudel, A., Bauer, H., Garcia, R.A.L., Biedrzycka, K., Khinast, J.G., 2020b. Developing HME-based drug products using emerging science: a fast-track roadmap from concept to clinical batch. AAPS PharmSciTech 21, 176. https://doi.org/10.1208/s12249-020-01713-0.
Matić, J., Witschnigg, A., Zagler, M., Eder, S., Khinast, J., 2019. A novel in silico scale-up approach for hot melt extrusion processes. Chem. Eng. Sci. 204, 257–269. https://doi.org/10.1016/j.ces.2019.04.016.
McFall, H., Sarabu, S., Shankar, V., Bandari, S., Murthy, S.N., Kolter, K., Langley, N., Kim, D.W., Repka, M.A., 2019. Formulation of aripiprazole-loaded pH-modulated solid dispersions via hot-melt extrusion technology: in vitro and in vivo studies. Int. J. Pharm. 554, 302–311. https://doi.org/10.1016/j.ijpharm.2018.11.005.
Menges, G., Feistkorn, W., 1984. Scale-up of twin screw extruders application and verification with the example of PVC. Adv. Polym. Technol. 4, 123–129. https://doi.org/10.1002/adv.1984.060040204.
Menges, G., Wortberg, J., Mayer, A., 1983. Model theory—an approach to design series of single-screw extruders. Adv. Polym. Technol. 3, 157–165. https://doi.org/10.1002/adv.1983.060030210.
Mishra, V., Thakur, S., Patil, A., Shukla, A., 2018. Quality by design (QbD) approaches in current pharmaceutical set-up. Expert Opin. Drug Deliv. 15, 737–758. https://doi.org/10.1080/17425247.2018.1504768.
Monaghan, J.J., 1992. Smoothed particle hydrodynamics. Annu. Rev. Astron. Astrophys. 30, 543–574. https://doi.org/10.1146/annurev.aa.30.090192.002551.
Monaghan, J.J., 1994. Simulating free surface flows with SPH. J. Comput. Phys. 110, 399–406. https://doi.org/10.1006/jcph.1994.1034.
Monaghan, J.J., 2000. SPH without a tensile instability. J. Comput. Phys. 159, 290–311. https://doi.org/10.1006/jcph.2000.6439.
Monaghan, J.J., 2005. Smoothed particle hydrodynamics. Rep. Prog. Phys. 68, 1703–1759. https://doi.org/10.1088/0034-4885/68/8/R01.
Monaghan, J.J., 2012. Smoothed particle hydrodynamics and its diverse applications. Annu. Rev. Fluid Mech. 44, 323–346. https://doi.org/10.1146/annurev-fluid-120710-101220.
Monaghan, J.J., Kajtar, J.B., 2009. SPH particle boundary forces for arbitrary boundaries. Comput. Phys. Commun. 180, 1811–1820. https://doi.org/10.1016/j.cpc.2009.05.008.
Morris, J.P., Fox, P.J., Zhu, Y., 1997. Modeling low reynolds number incompressible flows using SPH. J. Comput. Phys. 136, 214–226. https://doi.org/10.1006/jcph.1997.5776.
Mustafin, R.I., 2011. Interpolymer combinations of chemically complementary grades of Eudragit copolymers: a new direction in the design of peroral solid dosage forms of drug delivery systems with controlled release (review). Pharm. Chem. J. 45, 285–295. https://doi.org/10.1007/s11094-011-0618-7.
Parikh, T., Gupta, S.S., Meena, A., Serajuddin, A.T.M., 2014. Investigation of thermal and viscoelastic properties of polymers relevant to hot melt extrusion - III: Polymethacrylates and polymethacrylic acid based polymers. J. Excipients Food Chem. 5, 56–64.
Patil, H., Feng, X., Ye, X., Majumdar, S., Repka, M.A., 2015. Continuous production of fenofibrate solid lipid nanoparticles by hot-melt extrusion technology: a systematic study based on a quality by design approach. AAPS J. 17, 194–205. https://doi.org/10.1208/s12248-014-9674-8.
Pawlowski, J., 1971. Die Ähnlichkeitstheorie in der physikalisch-technischen Forschung, Springer Berlin Heidelberg, Berlin, Heidelberg. https://doi.org/10.1007/978-3-642-65095-6.
Perpétuo, G.L., Gálico, D.A., Fugita, R.A., Castro, R.A.E., Eusébio, M.E.S., Treu-Filho, O., Silva, A.C.M., Bannach, G., 2013. Thermal behavior of some antihistamines. J. Therm. Anal. Calorim. 111, 2019–2028. https://doi.org/10.1007/s10973-012-2247-0.
Rauwendaal, C., 2014. Polymer extrusion, Fifth edition. Carl Hanser Verlag GmbH & Co, KG, München. https://doi.org/10.3139/9781569905395.
Repka, M.A., Bandari, S., Kallakunta, V.R., Vo, A.Q., McFall, H., Pimparade, M.B., Bhagurkar, A.M., 2018. Melt extrusion with poorly soluble drugs – an integrated review. Int. J. Pharm. 535, 68–85. https://doi.org/10.1016/j.ijpharm.2017.10.056.
Repka, M.A., Battu, S.K., Upadhye, S.B., Thumma, S., Crowley, M.M., Zhang, F., Martin, C., McGinity, J.W., 2007. Pharmaceutical applications of hot-melt extrusion: Part II. Drug Dev. Ind. Pharm. 33, 1043–1057. https://doi.org/10.1080/03639040701525627.
Schittny, A., Ogawa, H., Huwyler, J., Puchkov, M., 2018. A combined mathematical model linking the formation of amorphous solid dispersions with hot-melt-extrusion process parameters. Eur. J. Pharm. Biopharm. 132, 127–145. https://doi.org/10.1016/j.ejpb.2018.09.011.

Siegmann, E., Jajcevic, D., Radeke, C., Strube, D., Friedrich, K., Khinast, J.G., 2017. Efficient discrete element method simulation strategy for analyzing large-scale agitated powder mixers. Chem. Ing. Tech. 89, 995–1005. https://doi.org/10.1002/cite.201700004.

Silva, L.A.D., Almeida, S.L., Alonso, E.C.P., Rocha, P.B.R., Martins, F.T., Freitas, L.A.P., Taveira, S.F., Cunha-Filho, M.S.S., Marreto, R.N., 2018. Preparation of a solid self-microemulsifying drug delivery system by hot-melt extrusion. Int. J. Pharm. 541, 1–10. https://doi.org/10.1016/j.ijpharm.2018.02.020.

Toson, P., Siegmann, E., Trogrlic, M., Kureck, H., Khinast, J., Jajcevic, D., Doshi, P., Blackwood, D., Bonnassieux, A., Daugherity, P.D., Am Ende, M.T., 2018. Detailed modeling and process design of an advanced continuous powder mixer. Int. J. Pharm. 552, 288–300. https://doi.org/10.1016/j.ijpharm.2018.09.032.

Treffer, D., Troiss, A., Khinast, J.G., 2015. A novel tool to standardize rheology testing of molten polymers for pharmaceutical applications. Int. J. Pharm. 495, 474–481. https://doi.org/10.1016/j.ijpharm.2015.09.001.

Vasoya, J.M., Desai, H.H., Gumaste, S.G., Tillotson, J., Kelemen, D., Dalrymple, D.M., Serajuddin, A.T.M., 2019. Development of solid dispersion by hot melt extrusion using mixtures of polyoxylglycerides with polymers as carriers for increasing dissolution rate of a poorly soluble drug model. J. Pharm. Sci. 108, 888–896. https://doi.org/10.1016/j.xphs.2018.09.019.

Viciosa, M.T., Moura Ramos, J.J., Diogo, H.P., 2016. The slow relaxation dynamics in the amorphous pharmaceutical drugs cimetidine, nizatidine, and famotidine. J. Pharm. Sci. 105, 3573–3584. https://doi.org/10.1016/j.xphs.2016.08.019.

Vo, A.Q., Feng, X., Morott, J.T., Pimparade, M.B., Tiwari, R.V., Zhang, F., Repka, M.A., 2016. A novel floating controlled release drug delivery system prepared by hot-melt extrusion. Eur. J. Pharm. Biopharm. 98, 108–121. https://doi.org/10.1016/j.ejpb.2015.11.015.

Wahl, P.R., Hörl, G., Kaiser, D., Sacher, S., Rupp, C., Shlieout, G., Breitenbach, J., Koscher, G., Khinast, J.G., 2018. In-line measurement of residence time distribution in melt extrusion via video analysis. Polym. Eng. Sci. 58, 170–179. https://doi.org/10.1002/pen.24544.

Yu, L.X., Amidon, G., Khan, M.A., Hoag, S.W., Polli, J., Raju, G.K., Woodcock, J., 2014. Understanding pharmaceutical quality by design. AAPS J. 16, 771–783. https://doi.org/10.1208/s12248-014-9598-3.

Zhu, Y., Shah, N.H., Waseem Malick, A., Infeld, M.H., McGinity, J.W., 2006. Controlled release of a poorly water-soluble drug from hot-melt extrudates containing acrylic polymers. Drug Dev. Ind. Pharm. 32, 569–583. https://doi.org/10.1080/03639040500528996.